Chin. Phys. B Vol. 30, No. 5 (2021) 054206

Dissipative Kerr solitons in optical microresonators with Raman effect and third-order dispersion*

Chaohua Wu(吴超华)[1,2], Zhiwei Fang(方致伟)[3,†], Jintao Fan(樊景涛)[1,2,‡], Gang Chen(陈刚)[1,2,4], and Ya Cheng(程亚)[2,3]

[1] State Key Laboratory of Quantum Optics and Quantum Optics Devices, Institute of Laser Spectroscopy, Shanxi University, Taiyuan 030006, China
[2] Collaborative Innovation Center of Extreme Optics, Shanxi University, Taiyuan 030006, China
[3] The Extreme Optoelectromechanics Laboratory (XXL), School of Physics and Materials Science, East China Normal University, Shanghai 200241, China
[4] Collaborative Innovation Center of Light Manipulations and Applications, Shandong Normal University, Jinan 250358, China

(Received 21 September 2020; revised manuscript received 2 December 2020; accepted manuscript online 8 December 2020)

Using the mean-field normalized Lugiato–Lefever equation, we theoretically investigate the dynamics of cavity soliton and comb generation in the presence of Raman effect and the third-order dispersion. Both of them can induce the temporal drift and frequency shift. Based on the moment analysis method, we analytically obtain the temporal and frequency shift, and the results agree with the direct numerical simulation. Finally, the compensation and enhancement of the soliton spectral between the Raman-induced self-frequency shift and soliton recoil are predicted. Our results pave the way for further understanding the soliton dynamics and spectral characteristics, and providing an effective route to manipulate frequency comb.

Keywords: dissipative Kerr soliton, frequency comb, Raman effect, dispersive wave

PACS: 42.65.−k, 78.47.jh **DOI:** 10.1088/1674-1056/abd15f

1. Introduction

Dissipative Kerr cavity solitons (DKS) are self-localized optical pulses that can be generated in nonlinear microresonators.[1–3] They come from a double balance between nonlinearity and dispersion as well as the parametric gain and cavity losses, which result in a stable pulse circulating within the cavity.[4] Recently, DKS have attracted significant research interest in the context of microresonator-based frequency comb generation, which have been demonstrated as a promising candidate for numerous applications, such as telecommunications,[5,6] frequency synthesis,[7] dual-comb spectroscopy,[8,9] astro-spectrometer calibration,[10,11] and optical atomic clocks.[12] These DKS-based frequency combs have been demonstrated in microresonators made of silica,[13–15] magnesium fluoride,[3,16] lithium niobate,[17] and silicon nitride.[18–20] In addition, such driven nonlinear microresonators are attractive platform for exploring spatiotemporal light localization and the dynamics of nonlinear systems.[21,22]

Typical description of the dynamics of cavity solitons is the mean-field Lugiato–Lefever equation (LLE) which usually excludes higher-order dispersion and nonlinear terms.[23,24] However in realistic system, higher-order effects are inevitable and can alter soliton properties significantly under certain conditions. Specifically, in the presence of higher-order dispersion, optical solitons can emit dispersive waves (soliton Cherenkov radiation), which provides a path to generate coherent broadband frequency combs.[25–29] This radiation process induces soliton recoil which causes a frequency shift in the spectral centre of the soliton. Furthermore, femtosecond solitons in microresonators have intense peak power and ultrashort duration such that, in principle, higher-order nonlinear effects like the self-steeping effect and intrapulse Raman scattering[30–32] can be excited. It has been demonstrated that soliton interaction with the Raman effect can induce soliton self-frequency redshift for a microresonator DKS (frequency-locked Raman soliton).[33–36] Thus, it is interesting to study the dynamics of cavity soliton and comb generation in the presence of both higher-order dispersion effects and Raman effect.

Here, we theoretically investigate the influence of Raman effect and the third-order dispersion on the dynamics of DKS. Specifically, we obtain approximated analytical expression of the temporal soliton drift and frequency shift based on the moment analysis method, which agrees with the numerical results according to directly solving the modified LLE. Furthermore, we predict the compensation and enhancement of the temporal and frequency shift in the presence of both the Raman effect and the third-order dispersion.

This work is organized as follows. Section 2 gives the

*Project supported by the National Key Research and Development Program of China (Grant Nos. 2017YFA0304203 and 2019YFA0705000), the National Natural Science Foundation of China (Grant Nos. 12004116 and 11804204), and 1331KSC.

†Corresponding author. E-mail: zwfang@phy.ecnu.edu.cn

‡Corresponding author. E-mail: bkxyfjt@163.com

mean-field normalized LLE. Section 3 describes the moment analysis method used in this work. Section 4 discusses the cavity soliton temporal drift and frequency shift under the Raman and the third-order dispersion effects.

2. Mean-field model

We describe the comb generation dynamics (schematically represented in Fig. 1) using the modified LLE, which incorporates terms of higher-order dispersion and the Raman effect. The equation can be written as[30,34,36,37]

$$\begin{aligned}\frac{\partial A(\phi,t)}{\partial t} =& -\left(\frac{\kappa}{2}+\mathrm{i}\delta\omega\right)A+\sum_{n\geq 2}(-\mathrm{i})^{n+1}\frac{D_n}{n!}\frac{\partial^n A}{\partial\phi^n}\\ &+S+\mathrm{i}g\left(|A|^2+D_1\tau_\mathrm{R}\frac{\partial|A|^2}{\partial\phi}\right)A,\end{aligned}\tag{1}$$

where $A(t,\phi)$ is the slowly varying intracavity field envelop, ϕ is the azimuthal angular coordinate inside the resonator, $\kappa=\kappa_0+\kappa_\mathrm{ex}$ is the sum of the intrinsic decay rate (κ_0) and the coupling rate to the waveguide (κ_ex), and $\eta=\kappa_\mathrm{ex}/\kappa$ is the coupling efficiency. The driving term $S=\sqrt{\kappa\eta P_\mathrm{in}/(\hbar\omega_0)}$, with P_in and ω_0 being the pump power and pumped resonance frequency, respectively. $\delta\omega=\omega_0-\omega_\mathrm{p}$ is the detuning of the pump laser with frequency ω_p. The nonlinear Kerr coupling coefficient is $g=\hbar\omega_0^2 cn_2/n_0^2V_\mathrm{eff}$, where n_0 and n_2 are respectively the linear and nonlinear refractive indices, and $V_\mathrm{eff}=A_\mathrm{eff}L$ is the effective optical mode volume (A_eff is the effective nonlinear optical mode area, and L is round-trip length of the microresonator). The last term in Eq. (1) denotes the Raman term, where τ_R is the Raman time constant. The resonance frequencies of one mode family in a microresonator can be approximated around ω_0 as a Taylor series $\omega_\mu=\omega_0+\sum_{n\geq 1}D_n\mu^n/n!$, where $\mu\in Z$ is the relative mode number, $D_1/2\pi$ is the free range of the resonator, D_2 is associated with the group velocity dispersion (GVD) parameter β_2 via $D_2=-(c/n_0)D_1^2\beta_2$, and $D_3, D_4,\ldots$, account for to higher-order dispersion.

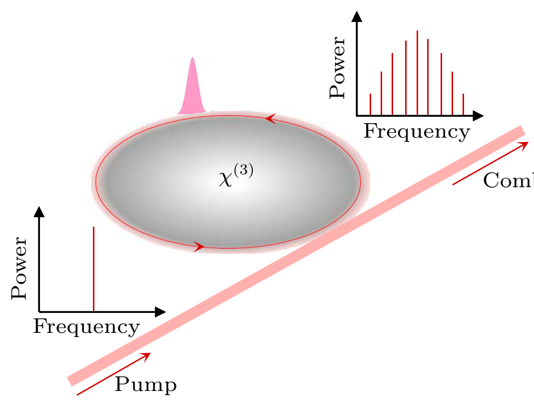

Fig. 1. Schematic diagram of Kerr optical frequency comb generation using nonlinear microresonator with $\chi^{(3)}$–Kerr nonlinearity.

For simplicity, we employ the following dimensionless form of Eq. (1):

$$\begin{aligned}\frac{\partial\psi(\theta,\tau)}{\partial\tau} =& -(1+\mathrm{i}\zeta)\psi+\sum_{n\geq 2}(-\mathrm{i})^{n+1}d_n\frac{\partial^n\psi}{\partial\theta^n}\\ &+\mathrm{i}|\psi|^2\psi+\mathrm{i}\tau_\mathrm{R}'\psi\frac{\partial|\psi|^2}{\partial\theta}+F.\end{aligned}\tag{2}$$

Here we have used the normalization convention $\tau=\kappa t/2$, $\theta=\phi\sqrt{\kappa/D_2}$, $\psi=\sqrt{2g/\kappa}A$, $d_n=\frac{2}{\kappa}(\kappa/|D_2|)^{n/2}\frac{D_n}{n!}$, $\zeta=2\delta\omega/\kappa$, $\tau_\mathrm{R}'=D_1\sqrt{\kappa/D_2}\tau_\mathrm{R}$, and $F=\sqrt{8g\eta P_\mathrm{in}/(\kappa^2\hbar\omega_0)}$. In the following analysis, we focus on the abnormal dispersion, *i.e.*, $d_2=1$.

3. Moment analysis

To quantitatively understand the dynamics of the DKS described by Eq. (2), we first use the method of moments to search the approximate soliton solutions. The moment analysis method treats the pulse as a particle, under which the energy $\mathcal{E}$, position $\mathcal{D}$, and the spectral centre mode number μ_c are given by[34,36]

$$\mathcal{E}=\int_{-\infty}^{\infty}|\psi|^2\,\mathrm{d}\theta,\tag{3}$$

$$\mathcal{D}=\frac{1}{\mathcal{E}}\int_{-\infty}^{\infty}\theta|\psi|^2\,\mathrm{d}\theta,\tag{4}$$

$$\mu_\mathrm{c}=\frac{\mathrm{i}}{2\mathcal{E}}\int_{-\infty}^{\infty}\left(\psi^*\frac{\partial\psi}{\partial\theta}-\psi\frac{\partial\psi^*}{\partial\theta}\right)\mathrm{d}\theta.\tag{5}$$

Taking derivations of the moments Eqs. (3)–(5) and using Eq. (2), we get

$$\frac{\partial\mathcal{E}}{\partial\tau}=-2\mathcal{E}+F\int_{-\infty}^{\infty}(\psi+\psi^*)\,\mathrm{d}\theta,\tag{6}$$

$$\begin{aligned}\frac{\partial\mathcal{D}}{\partial\tau} =& -2\mathcal{D}+2\mu_\mathrm{c}+\frac{F}{\mathcal{E}}\int_{-\infty}^{\infty}\theta(\psi+\psi^*)\,\mathrm{d}\theta\\ &+\sum_{n>1}\int_{-\infty}^{\infty}(2n-1)\frac{d_{2n-1}}{\mathcal{E}}\left|\frac{\partial^{n-1}\psi}{\partial\theta^{n-1}}\right|^2\mathrm{d}\theta\\ &-\mathrm{i}\sum_{n>1}\int_{-\infty}^{\infty}\frac{nd_{2n}}{\mathcal{E}}[\psi,\psi^*]_n\,\mathrm{d}\theta,\end{aligned}\tag{7}$$

$$\frac{\partial\mu_\mathrm{c}}{\partial\tau}=-2\mu_\mathrm{c}+\frac{\tau_\mathrm{R}'}{\mathcal{E}}\int_{-\infty}^{\infty}\left(\frac{\partial|\psi|^2}{\partial\theta}\right)^2\mathrm{d}\theta,\tag{8}$$

where

$$[\psi,\psi^*]_k=\frac{\partial^{k-1}\psi^*}{\partial\theta^{k-1}}\frac{\partial^k\psi}{\partial\theta^k}-\frac{\partial^{k-1}\psi}{\partial\theta^{k-1}}\frac{\partial^k\psi^*}{\partial\theta^k}.$$

Considering $\mathcal{F}\left[\partial^k\psi(\tau,\theta)/\partial\theta^k\right]=(-\mathrm{i}\mu)^k\psi(\tau,\mu)$ and $\partial\left[(-\mathrm{i}\mu)^k\psi(\tau,\mu)\right]/\partial\tau=0$, where $\mathcal{F}$ denotes the Fourier transform, it follows that the temporal position shift of the soliton in Eq. (7) is dominated by high-odd-order dispersion (d_{2n+1}), and the high-even-order dispersion (d_{2n}) term only affects the relation between the width and the amplitude of the soliton.[26] Furthermore, the second term of Eq. (8) implies that the Raman effect can induce frequency shift.

4. Raman and third-order dispersion perturbation

We introduce the following soliton envelope ansatz[35,38]

$$\psi(\theta,\tau)=\sqrt{\frac{\mathcal{E}}{2\tau_{\rm s}}}\,{\rm sech}\left[\frac{\theta-\mathcal{D}(\tau)}{\tau_{\rm s}}\right]{\rm e}^{-{\rm i}\mu_{\rm c}(\tau)[\theta-\mathcal{D}(\tau)]+{\rm i}\varphi}, \quad (9)$$

with energy $\mathcal{E}$, temporal pulse width $\tau_{\rm s}$, temporal position $\mathcal{D}$, spectral-center frequency shift $\mu_{\rm c}$, and soliton phase φ. By substituting Eq. (9) into Eqs. (6)–(8) and taking into consideration the dispersion up to the third order, we obtain

$$\frac{\partial\mathcal{E}}{\partial\tau}=-2\mathcal{E}+2\pi F\sqrt{\frac{\mathcal{E}\tau_{\rm s}}{2}}\,{\rm sech}\left(\frac{\pi\mu_{\rm c}\tau_{\rm s}}{2}\right)\cos\varphi, \quad (10)$$

$$\frac{\partial\mathcal{D}}{\partial\tau}=-2\mathcal{D}+2\mu_{\rm c}+2\pi F\mathcal{D}\tau_{\rm s}\sqrt{\frac{1}{2\mathcal{E}\tau_{\rm s}}}\,{\rm sech}\left(\frac{\pi\mu_{\rm c}\tau_{\rm s}}{2}\right)\cos\varphi+\frac{3d_3}{\tau_{\rm s}}\left(\frac{1}{3\tau_{\rm s}}+\mu_{\rm c}^2\tau_{\rm s}\right), \quad (11)$$

$$\frac{\partial\mu_{\rm c}}{\partial\tau}=-2\mu_{\rm c}-\frac{4}{15}\frac{\mathcal{E}}{\tau_{\rm s}^3}\tau_{\rm R}'. \quad (12)$$

In the unperturbed case ($d_3=0$, $\tau_{\rm R}'=0$), the stability analysis of the equilibrium intracavity field $\psi_{\rm s}$ of Eq. (2) fulfills the cubic equation $F^2=\rho^3-2\zeta\rho^2+(\zeta^2+1)\rho$, where $\rho=|\psi_{\rm s}|^2$. From Eq. (10), the steady-state energy ($\partial\mathcal{E}/\partial\tau=0$) of the unperturbed cavity soliton is obtained by assuming $\cos\varphi\approx1$. That is $\mathcal{E}_0\approx\pi^2F^2\tau_{\rm s0}/2$ and the temporal pulse width is $\tau_{\rm s0}\approx\mathcal{E}_0/4$.[38] From Eqs. (11) and (12) we have $\mathcal{D}=0$ and $\mu_{\rm c}=0$, meaning that the cavity soliton dose not move and keeps its initial frequency, as shown in Fig. 2(a). The field evolves toward a steady-state pulse [Fig. 2(b)] and the corresponding spectral is a perfectly smooth sech function [Fig. 2(c)].

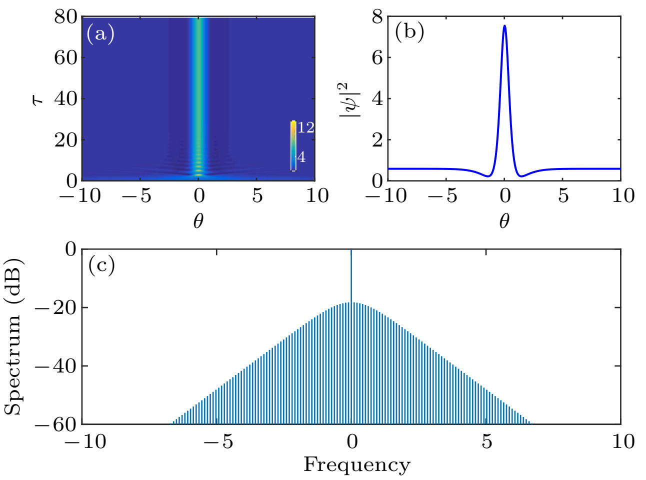

Fig. 2. (a) Temporal evolution of the cavity soliton for $\zeta=3$, $F=2$, and $d_3=\tau_{\rm R}'=0$. (b) Temporal and (c) spectral envelopes of the final stable soliton.

We first address the effect of Raman term ($d_3=0$, $\tau_{\rm R}'\neq0$). According to Eqs. (11) and (12), the steady-state spectral center mode number ($\partial\mu_{\rm c}/\partial\tau=0$) is given as

$$\mu_{\rm c,R}\approx-\frac{2}{15}\frac{\mathcal{E}_0}{\tau_{\rm s0}^3}\tau_{\rm R}', \quad (13)$$

and the temporal shift of the soliton is

$$\mathcal{D}_{\rm R}(\tau)\approx2\mu_{\rm c,R}\tau. \quad (14)$$

Here we have assumed ${\rm sech}(\pi\mu_{\rm c}\tau_{\rm s}/2)\cos\varphi\approx1$. In Figs. 3(a) and 3(b), by numerically solving Eq. (2), we plot the temporal and spectral evolutions of cavity soliton *versus* slow time τ, respectively, and the final steady state temporal and spectral envelops are shown in Figs. 3(c) and 3(d). It is clear that Raman effect induces a temporal deceleration and spectral redshift to the soliton. Moreover, equation (14) shows that the temporal shift $\mathcal{D}_{\rm R}(\tau)$ induced by the Raman effect varies linearly with τ [see Fig. 3(e)]. In Fig. 3(f) we plot $\mu_{\rm c,R}$ *versus* $\tau_{\rm R}'$. The analytical results agree well with the numerical calculation for small $\tau_{\rm R}'$. As $\tau_{\rm R}'$ is increased, the deviation will increase.

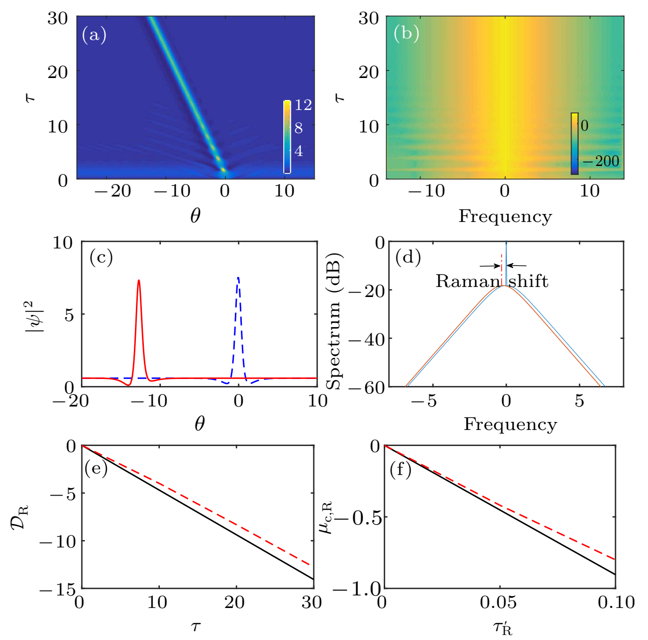

Fig. 3. Temporal (a) and spectral (b) evolutions of the cavity soliton for $\tau_{\rm R}'=0.04$. Panels (c) and (d) show the temporal and spectral envelopes. The blue curves in panels (c) and (d) correspond to Figs. 2(b) and 2(c), respectively. Panel (e) shows the temporal delay of the soliton *versus* slow time τ with $\tau_{\rm R}'=0.04$ and panel (f) shows the frequency shift *versus* $\tau_{\rm R}'$ with $\tau=30$. The red dashed lines correspond to numerical results by solving Eq. (2) and the black solid lines are the solutions of Eqs. (13) and (14), respectively. The other parameters are the same as those in Fig. 2.

We then study the impacts of the third-order dispersion ($d_3\neq0$, $\tau_{\rm R}'=0$). Equation (11) shows that the third-order dispersion influences the temporal position of the soliton and the position shift is

$$\mathcal{D}_{\rm T}(\tau)\approx\frac{d_3}{\tau_{\rm s0}^2}\tau. \quad (15)$$

This is clarified in Fig. 4(a1), which plots the temporal evolution dynamics of soliton with $d_3=0.1$. Furthermore, we plot the position shift $\mathcal{D}_{\rm T}$ *versus* time τ (with $d_3=0.1$) and d_3 (at time $\tau=50$), respectively. It is found that results from Eq. (15) (black solid lines) agrees with the numerical data (red dashed lines). Compared with the unperturbed case [Figs. 2(b) and

2(c)], the third-order dispersion induces soliton tail oscillation, as shown on the top of Fig. 4(a1). This originates from the dispersive wave excitation via Cherenkov radiation process. The corresponding spectrum of such a perturbed soliton exhibits an additional local maximum (dispersive wave), as shown in Fig. 4(a2). In addition, the sign of d_3 determines the direction of soliton movement and the side of dispersive wave, as shown in Figs. 4(b1) and 4(b2) with $d_3 = -0.1$.

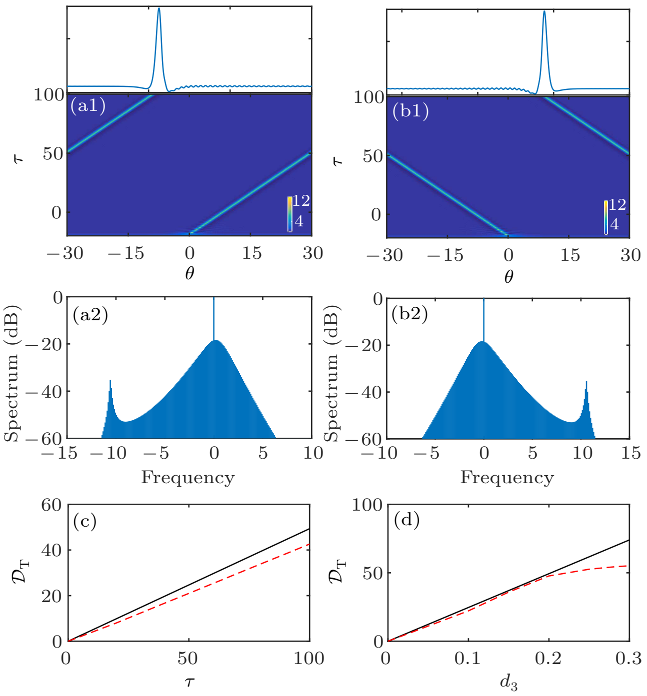

Fig. 4. Panels (a1) and (a2) [(b1) and (b2)] are the temporal and spectral evolutions of the cavity soliton for $d_3 = 0.1$ [$d_3 = -0.1$], respectively. The upper graph in panels (a1) and (b1) show the corresponding temporal profile of the stable evolution soliton. Panels (c) and (d) show the temporal delay of the soliton *versus* time τ with $d_3 = 0.1$ and Raman constant d_3 with $\tau = 50$, respectively. The red dashed lines correspond to numerical results by solving Eq. (2) and the black solid lines are the solutions of Eq. (15). The other parameters are the same as those in Fig. 2.

As shown in Fig. 5(a), owing to the appearance of the dispersive wave, the maximum of spectrum shifted away from the pump frequency, which is called soliton recoil. To estimate the peak position of the spectrum, we treat d_3 as a perturbation up to the first order, and the solution of Eq. (2) is thus given as[39]

$$\tilde{\psi} = \sqrt{2\zeta}\operatorname{sech}\left(\sqrt{\zeta}\Theta\right)\mathrm{e}^{\mathrm{i}\sqrt{\zeta}d_3 f(\Theta)}, \tag{16}$$

where $\Theta = \theta - d_3\zeta\upsilon\tau = \theta - (\partial\mathcal{D}/\partial\tau)\sqrt{\zeta}\tau$ and $f(\Theta) = [(\upsilon+1)\Theta - 3\tanh(\Theta)]/2$. Making use of Eq. (15), we have $\upsilon \approx 1$. Note that we have neglected some dispensable terms in writing Eq. (16) and focused on the frequency shift induced by the third-order dispersion. Taking the Fourier transform of Eq. (16), *i.e.*, $\mathcal{F}[\mathcal{A}(\mu)] = \int\mathcal{A}(\theta)\,\mathrm{e}^{-\mathrm{i}\mu\theta}\,\mathrm{d}\theta$, the soliton recoil is written as

$$\mu_{\mathrm{r}} \approx 2\sqrt{\zeta}d_3. \tag{17}$$

In Fig. 5(b), we plot soliton recoil *versus* d_3. It can be seen that the analytical results (black solid line) agree with the numerical simulation (red dashed line) for small d_3. Note that the obtained results may be more precise if higher-order correlations (nonlinear term) are considered. Additionally, according to the dispersive radiation theory,[27,40] the frequency of dispersive wave is $D_\omega = d_3\mu^3 - \nu\mu \pm \sqrt{(d_2\mu^2 + 2|\psi_0|^2 - \zeta)^2 - |\psi_0|^4}$, where ν is the velocity of the soliton temporal drift and $|\psi_0|^2$ is the background power. The peak position of the dispersive wave is obtained by setting $D_\omega = 0$. In the lower panel of Fig. 5(a), we plot the corresponding spectrum of dispersion wave. One can see that the dispersive wave is located at normal dispersion regime, which demonstrates a broadband frequency comb.

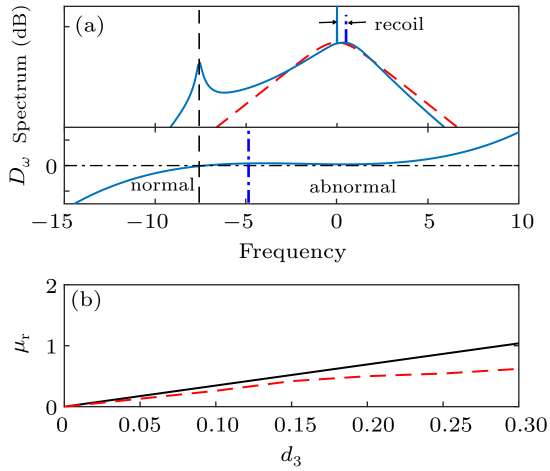

Fig. 5. (a) The spectral envelop (upper panel) and dispersive wave curve (lower panel) with $d_3 = 0.15$. The red dashed line corresponds to the envelop in Fig. 2(c). In the dispersive wave curve, regions with positive curvature have anomalous group velocity dispersion (GVD) and regions with negative curvature have normal GVD. Panel (b) shows the soliton recoil *versus* d_3 based on Eq. (17) (black solid line) and numerical results (red dashed line). The other parameters are the same as those in Fig. 2.

Up to now, the discussions are restricted to the case where either Raman term or the third-order dispersion is taken into consideration. Since both these terms are inevitable in an actual experiment, it becomes necessary to understand their potential interplay on the dynamics of DKS. Firstly, according to Eq. (11), both terms lead to temporal shift of the intracavity soliton. In Figs. 6(a) and 6(b), we plot the temporal evolution of the cavity soliton for $\{d_3 = 0.1, \tau_{\mathrm{R}}' = 0.04\}$ and $\{d_3 = -0.1, \tau_{\mathrm{R}}' = 0.04\}$, respectively. The white solid lines (red dashed lines) denote the temporal evolution profiles with $\{d_3 \neq 0, \tau_{\mathrm{R}}' = 0\}$ ($\{d_3 = 0, \tau_{\mathrm{R}}' \neq 0\}$). One can see that, under the action of both Raman effect and the third-order dispersion, the soliton temporal drift can be either compensated or enhanced depending on the sign of d_3. In particularly, the corresponding frequency shift can also be compensated or enhanced, as shown in Figs. 6(c) and 6(d). When $d_3 = 0.1$, the Raman induced soliton self-frequency shift cancels the soliton recoil induced by dispersive wave [inset in Fig. 6(c)]. For $d_3 = -0.1$, both Raman self-frequency shift and soliton recoil are attributed to the enhancement of frequency shift [inset in Fig. 6(d)]. We can eliminate the influence of the Raman effect by engineering the third-order dispersion of the microresonator. Note that, in addition to the soliton spectrum, the Raman term can also influence the position of the dispersive wave situated in the normal disperion regime.

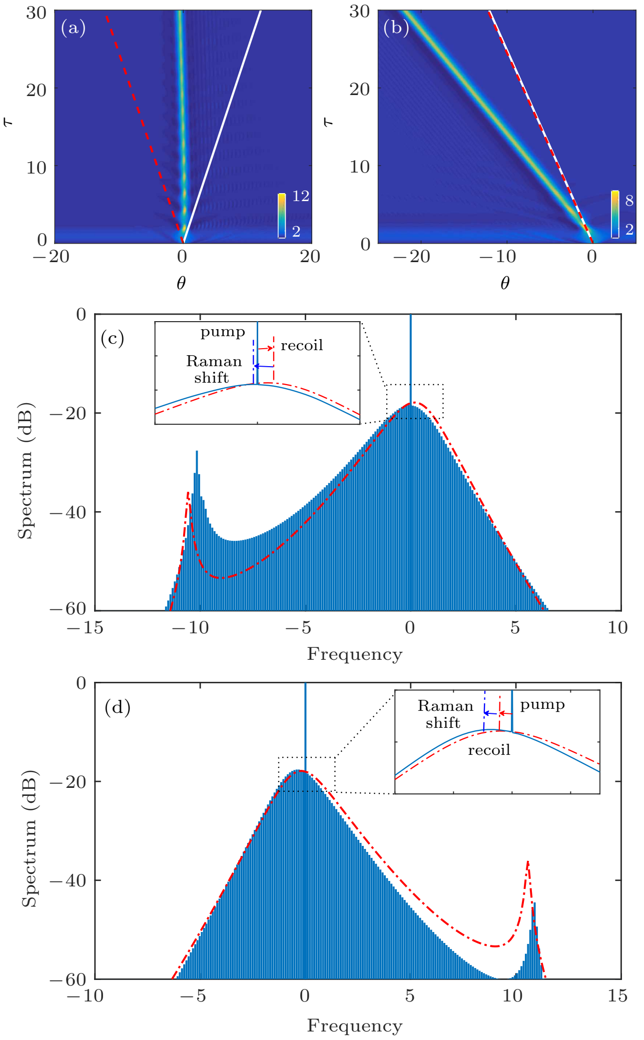

Fig. 6. Panels (a) and (b) show the temporal evolution of the cavity soliton for $\{d_3 = 0.1, \tau'_{\mathrm{R}} = 0.04\}$ and $\{d_3 = -0.1, \tau'_{\mathrm{R}} = 0.04\}$, respectively. The white solid (red dashed) lines represent the temporal evolution profiles with only d_3 (τ'_{R}). Panels (c) and (d) are the corresponding spectra in panels (a) and (b), respectively, and the red dotted–dashed lines denote the spectral profiles with $\{d_3 \neq 0, \tau'_{\mathrm{R}} = 0\}$. The other parameters are the same as those in Fig. 2.

5. Conclusion

In summary, we have studied the role of the Raman effect and the third-order dispersion in cavity soliton and frequency comb generation. Based on the mean-field LLE, we used the moment analysis method to describe the dynamics of cavity soliton. Particularly, we obtained approximated analytical expression for the temporal soliton drift and frequency shift under the Raman effect or the third-order dispersion. The analytical results for small Raman shock time and the third-order dispersion coefficient agree with full simulation by solving LLE numerically using the split-step Fourier method. Finally, we predict the cancellation and enhancement of the temporal drift and frequency shift in the presence of both the Raman effect and the third-order dispersion.

Appendix A: Raman effect

Note that the general Raman term in Eq. (1) is $\mathrm{i}g\int_0^\infty R(t')\,|A(\phi, t-t')|^2\,\mathrm{d}t'A$. Here $R(t) = (1-f_{\mathrm{R}})\,\delta(t) + f_{\mathrm{R}}h_{\mathrm{R}}(\phi)$ is the nonlinear response function, where f_{R} is the Raman fration and $h_{\mathrm{R}}(\phi)$ is the Raman response function. Thus, the Raman term is rewritten as $\mathrm{i}g\left[(1-f_{\mathrm{R}})\,|A|^2 + f_{\mathrm{R}}h_{\mathrm{R}}(\phi)\otimes|A|^2\right]A$, with $\otimes$ denoting convolution. Given that Raman-active modes are sufficiently high in frequency and exceed the bandwidth of the soliton pulse, then the Raman term can be simplified to the first order that only contains the instantaneous response, *i.e.*, $h_{\mathrm{R}}(\phi)\otimes|A|^2 \approx |A|^2 + D_1\tau_{\mathrm{R}}\partial|A|^2/\partial\phi$.

References

[1] Akhmediev N and Ankiewicz A 2008 *Dissipative Solitons: From Optics to Biology and Medicine* (Springer)
[2] Leo F, Coen S, Kockaert P, Gorza S P, Emplit P and Haelterman M 2010 *Nat. Photon.* **4** 471
[3] Herr T,Brasch V, Jost J D, Wang C Y, Kondratiev N M, Gorodetsky M L and Kippenberg T J 2014 *Nat. Photon.* **8** 145
[4] Kippenberg T J, Gaeta A L, Lipson M and Gorodetsky M L 2018 *Science* **361** eaan8083
[5] Chen J W, Wang J D, Qu X H and Zhang F M 2019 *Acta Phys. Sin.* **68** 190602 (in Chinese)
[6] Marin-Palomo P, Kemal J N, Karpov M, Kordts A, Pfeifle J, Pfeiffer M H P, Trocha P, Wolf S, Brasch V, Anderson M H, Rosenberger R, Vijayan K, Freude W, Kippenberg T J and Koos C 2017 *Nature* **546** 274
[7] Spencer D T, Drake T, Briles T C, Stone J, Sinclair L C, Fredrick C, Li Q, Westly D, Ilic B R, Blue stone A, Volet N, Komljenovic T, Chang L, Lee S H, Oh D Y , Suh M G, Yang K Y, Pfeiffer M H P, Kippenberg T J, Norberg E, Theogarajan L, Vahala K, Newbury N R, Srinivasan K, Bowers J E, Diddams S A and Papp S B 2018 *Nature* **557** 81
[8] Suh M G, Yang Q F, Yang K Y, Yi X and Vahala K J 2016 *Science* **354** 600
[9] Dutt A, Joshi C, Ji X, Cardenas J, Okawachi Y, Luke K, Gaeta A L and Lipson M 2018 *Sci. Adv.* **4** e1701858
[10] Obrzud E, Rainer M, Harutyunyan A, Anderson M H, Liu J, Geiselmann M, Chazelas B, Kundermann S, Lecomte S, Cecconi M, Ghedina A, Molinari E, Pepe F, Wildi F, Bouchy F, Kippenberg T J and Herr T 2019 *Nat. Photon.* **13** 31
[11] Suh M G, Yi X, Lai Y H, Leifer S, Grudinin I S, Vasisht G, Martin E C, Fitzgerald M P, Doppmann G, Wang J, Mawet D, Papp S B, Diddams S A, Beichman C and Vahala K 2019 *Nat. Photon.* **13** 25
[12] Newman Z L, Maurice V, Drake T, Stone J R, Briles T C, Spencer D T, Fredrick C, Li Q, Westly D, Ilic B R, Shen B, Suh M G, Yang K Y, Johnson C, Johnson D M S, Hollberg L, Vahala K J, Srinivasan K, Diddams S A, Kitching J, Papp S B and Hummon M T 2019 *Optica* **6** 680
[13] Yi X, Yang Q F, Yang K Y, Suh M G and Vahala K 2015 *Optica* **2** 1078
[14] Cole D C, Lamb E S, Del'Haye P, Diddams S A and Papp S B 2017 *Nat. Photon.* **11** 671
[15] Chen H J, Ji Q X, Wang H, Yang Q F, Cao Q T, Gong Q, Yi X and Xiao Y F 2020 *Nat. Commun.* **11** 2336
[16] Guo H, Karpov M,Lucas E, Kordts A, Pfeiffer M H P, Brasch V, Lihachev G, Lobanov V E, Gorodetsky M L and Kippenberg T J 2017 *Nat. Phys.* **13** 94
[17] He Y, Yang Q F, Ling J, Luo R, Liang H, Li M, Shen B, Wang H, Vahala K and Lin Q 2019 *Optica* **6** 1138
[18] Joshi C, Jang J K, Luke K, Ji X, Miller S A, Klenner A, Okawachi Y, Lipson M and Gaeta A L 2016 *Opt. Lett.* **41** 2565

[19] Wang P H, Jaramillo-Villegas J A, Xuan Y, Xue X, Bao C, Leaird D E, Qi M and Weiner A M 2016 *Opt. Express* **24** 10890

[20] Wan S, Niu R, Wang Z Y, Peng J L, Li M, Li J, Guo G C, Zou C L and Dong C H 2020 *Photon. Res.* **8** 1342

[21] Anderson M, Wang Y, Leo F, Coen S, Erkintalo M and Murdoch S G 2017 *Phys. Rev. X* **7** 031031

[22] Wu C, Fan J, Chen G and Jia S 2019 *Opt. Express* **27** 028133

[23] Chembo Y K and Menyuk C R 2013 *Phys. Rev. A* **87** 053852

[24] Xu X, Jin X Y, Hu X H and Huang X N 2020 *Acta Phys. Sin.* **69** 024203 (in Chinese)

[25] Coen S, Randle H G, Sylvestre T and Erkintalo M 2013 *Opt. Lett.* **38** 37

[26] Wang S, Guo H, Bai X and Zeng X 2014 *Opt. Lett.* **39** 2880

[27] Milián C and Skryabin D V 2014 *Opt. Express* **22** 3732

[28] Brasch V, Geiselmann M, Herr T, Lihachev G, Pfeiffer M H P, Gorodetsky M L and Kippenberg T J 2016 *Science* **351** 357

[29] Liu M, Wang L, Sun Q, Li S, Ge Z, Lu Z, Zeng C, Wang G, Zhang W, Hu X and Zhao W 2018 *Opt. Express* **26** 016477

[30] Okawachi Y, Yu M, Venkataraman V, Latawiec P M, Griffith A G, Lipson M, Loncar M and Gaeta A L 2017 *Opt. Lett.* **42** 2786

[31] Bao C, Xuan Y, Wang C, Jaramillo-Villegas J A, Leaird D E, Qi M and Weiner A M 2017 *Opt. Lett.* **42** 759

[32] Fang Z, Luo H, Lin J, Wang M, Zhang J, Wu R, Zhou J, Chu W, Lu T and Cheng Y 2019 *Opt. Lett.* **44** 5953

[33] Milián C, Gorbach A. V, Taki M, Yulin A V and Skryabin D V 2015 *Phys. Rev. A* **92** 033851

[34] Karpov M, Guo H, Kordts A,Brasch V, Pfeiffer M H P, Zervas M, Geiselmann M and Kippenberg T J 2016 *Phys. Rev. Lett.* **116** 103902

[35] Yi X, Yang Q F, Yang K Y and Vahala K 2016 *Opt. Lett.* **41** 003419

[36] Yi X, Yang Q F, Zhang X, Yang K Y, Li X and Vahala K 2017 *Nat. Commun.* **8** 14869

[37] Wang J, Sheng A G, Huang X, Li R Y and He G Q 2020 *Chin. Phys. B* **29** 034207

[38] Sahoo A and Roy S 2019 *Phys. Rev. A* **100** 053814

[39] Cherenkov A V, Lobanov V E and Gorodetsky M L 2017 *Phys. Rev. A* **95** 033810

[40] Malaguti S, Conforti M and Trillo S 2014 *Opt. Lett.* **39** 5626